

Cite this article as: Zhao Guangxi, Cheng Xiang, Yang Xianhai, et al. Numerical Analysis of Ripple Formation Process During Pulsed TIG Welding[J]. Rare Metal Materials and Engineering, 2023, 52(01): 133-138.

ARTICLE

Numerical Analysis of Ripple Formation Process During Pulsed TIG Welding

Zhao Guangxi^{1,2,3}, Cheng Xiang¹, Yang Xianhai¹, Zheng Guangming¹, Liu Huanbao¹, Tan Shuai²

¹School of Mechanical Engineering, Shandong University of Technology, Zibo 255000, China; ²Shengli Oilfield Highland Petroleum Equipment Co., Ltd, Dongying 257091, China; ³Shandong Provincial Key Laboratory of Precision Manufacturing and Non-traditional Machining, Zibo 255000, China

Abstract: With the consideration of the influence of arc driving forces, a 3D transient numerical model was established for the ripple formation process during pulsed tungsten inert gas (TIG) welding. To avoid the influence of droplet caused by the melting of welding wire on the surface fluctuation of molten pool, the wire-feeding process did not proceed when the arc was scanning the 2024 aluminum alloy substrate. Results show that the molten pool surface fluctuates periodically when the current is switched between the base value and the peak value. With the arc movement, the rear side of molten pool is solidified gradually. The molten pool surface is solidified before flattening under the cooling with large temperature gradient, resulting in the welding ripples. The formation frequency of the welding ripples is equal to the current pulse frequency. The distance between adjacent welding ripples is approximately equal to the product of the arc scanning velocity and the current pulse frequency.

Key words: ripple formation; TIG welding; molten pool; arc driving force

Tungsten inert gas (TIG) welding is widely used in metal joining, additive manufacture, workpiece preheating, and other fields due to its low cost, high productivity, and easy operation^[1-2]. However, the application of TIG welding is restricted by the surface defects, such as ripples, undercutting, and humping. The mechanism of ripple formation is crucial to the accuracy, quality, and reliability of welding^[3-4].

The formation of ripples is attributed to the dynamics of the molten pool with periodic oscillations during the solidification process. Unni^[5], Sharma^[6], Huang^[7], and Chen^[8] et al investigated the temperature distribution and the dynamics of TIG weld pool without consideration of the effect of arc forces on the surface morphology. The welding ripples are neglected in those researches. Sagar et al^[9] studied the temperature distribution during TIG welding by the element birth and death model in ANSYS software. Mohanty et al^[10] developed a new heat source model to simulate the alternating current square wave welding, and found that the welding surface after solidification is smooth without welding ripples.

Meng et al^[11] studied the influence of sensitivity of driving forces on the weld pool behavior. The formation of welding ripples is complex and depends on the process parameters. The influence of arc driving forces on the molten pool morphology has been studied, but the formation process of welding ripple is not thoroughly investigated^[12-14]. Wei et al^[15] studied the surface ripple amplitude and found that the average amplitude is proportional to the surface pressure of the molten pool. Liu et al^[16] studied the weld pool dynamics and found that the high peak current corresponds to the high ripples and deep penetration. Liang et al^[17] studied the ripple formation in dissimilar welding under the pulsed laser, and reported that the higher the pulsed frequency, the smoother the surface. Yao et al^[18] demonstrated that the ripple formation process can reflect the quality of the welding process. Generally, the welding ripples are mainly caused by the periodic impact of droplets generated by the molten welding wire^[19-20]. However, the welding ripples can also be generated when the wire-feeding process does not proceed.

Received date: April 04, 2022

Foundation item: National Natural Science Foundation of China (52075306)

Corresponding author: Zhao Guangxi, Ph. D., School of Mechanical Engineering, Shandong University of Technology, Zibo 255000, P. R. China, E-mail: zgx2019@sdut.edu.cn

Copyright © 2023, Northwest Institute for Nonferrous Metal Research. Published by Science Press. All rights reserved.

A three-dimensional transient welding model was developed to simulate the ripple formation process for the moving pulsed TIG welding without wire-feeding. This research discussed the formation mechanism of surface ripples for optimization of process parameters.

1 Mathematical Model Establishment

1.1 Heat source and arc driving force

The influence of heat source movement and penetration depth on the heat flow distribution was considered in the double ellipsoid heat source model, resulting in higher accuracy than that of the Gaussian heat source model^[21]. The heat flux of double ellipsoid heat source model could be divided into two parts^[22], as expressed by Eq.(1) and Eq.(2), as follows:

$$q_f(x,y,z) = \frac{f_f \eta UI 6 \sqrt{3}}{\pi \sqrt{\pi} a_f bc} \exp \left[-3 \left(\frac{x}{a_f} \right)^2 - 3 \left(\frac{y}{b} \right)^2 - 3 \left(\frac{z}{c} \right)^2 \right] \quad (1)$$

$$q_r(x,y,z) = \frac{f_r \eta UI 6 \sqrt{3}}{\pi \sqrt{\pi} a_r bc} \exp \left[-3 \left(\frac{x}{a_r} \right)^2 - 3 \left(\frac{y}{b} \right)^2 - 3 \left(\frac{z}{c} \right)^2 \right] \quad (2)$$

where f_f and f_r are energy distribution coefficients with $f_f + f_r = 2$; U and I are welding voltage and current, respectively; η is the absorption rate of welding heat energy of the material; a_f and a_r are the length of the front and back semi-axes of the ellipse, respectively; b is the half width of molten pool; c is the half depth of molten pool; x , y , and z are the coordinate positions.

According to the generation principle of driving forces, the arc pressure, surface tension, and drag force are all surface forces, which affect the weld pool surface. Buoyancy and Lorentz force are the volume forces, which affect the whole weld pool, as shown in Fig.1. The buoyancy is caused by the density variation of aluminum alloy which results from the temperature change^[23], as expressed by Eq.(3), as follows:

$$F_b = -\rho_0 \alpha (T - T_0) g \quad (3)$$

where α is the linear expansion coefficient of the material; ρ_0 is the aluminum alloy density at the reference temperature T_0 (T_0 is usually equal to room temperature); T represents the fluid temperature; g is the gravitational acceleration.

The relationship between arc pressure and coordinate position can be expressed by Gaussian equation^[24], as follows:

$$p_{\text{arc}} = \frac{\mu_0 I^2}{4\pi r_A^2} \exp \left(-\frac{x^2 + y^2}{2r_A^2} \right) \quad (4)$$

where μ_0 represents the magnetic permeability of space with $\mu_0 = 1.26 \times 10^{-6}$ H/m; r_A is the effective radius of welding arc acting on the upper surface of the substrate. The control equations of other driving forces are obtained based on Ref.[25–26].

1.2 Numerical model

The schematic diagram of boundary conditions and mesh of the 3D numerical model is shown in Fig. 2. In order to simplify the calculation, a symmetry boundary was adopted on the xz plane. The initial position of the arc center was at the junction of the symmetry plane and the upper surface of the substrate, and the arc center moved at a speed of 8 mm/s along the x axis. The control equations of the heat flux and arc driving forces were compiled by the Fortran language programming. The volume of fluid (VOF) method^[27] was used to track the free interface of the molten pool. In addition, the heat conduction, heat convection, and heat radiation were all considered during the calculation of welding process^[28]. The 2024 aluminum alloy was adopted as the substrate material, and its thermophysical properties are shown in Table 1.

The distance between the substrate and tungsten electrode was 4 mm. The variation of pulse current I and voltage V with time t is shown in Fig.3. The pulse current frequency was 5 Hz, the peak current was 200 A, and the base current was 100 A. The voltages corresponding to the peak current and base current are 18.2 and 14.5 V, respectively. The arc shapes corresponding to the base current and peak current are shown in Fig. 4. The initial temperature of the substrate and the environment was 298 K.

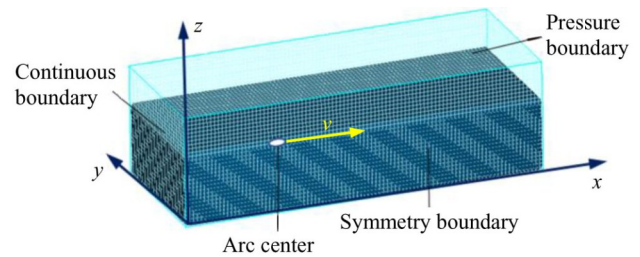


Fig.2 Schematic diagram of boundary conditions and mesh of 3D numerical model

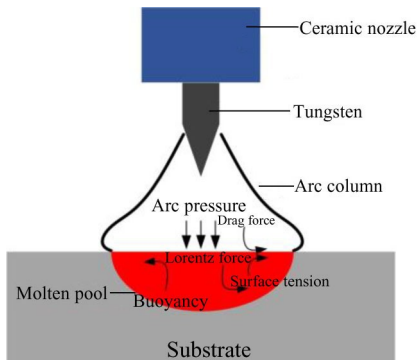


Fig.1 Distribution of arc driving forces in molten pool

Table 1 Thermophysical properties of 2024 aluminum alloy

Property	Value
Specific heat/ $J \cdot (kg \cdot K)^{-1}$	850
Thermal conductivity/ $W \cdot (m \cdot K)^{-1}$	175
Solidifying point/K	811.5
Melting point/K	905.5
Liquid density/ $kg \cdot m^{-3}$	2640
Solid density/ $kg \cdot m^{-3}$	2785
Viscosity/ $kg \cdot (m \cdot s)^{-1}$	0.0013

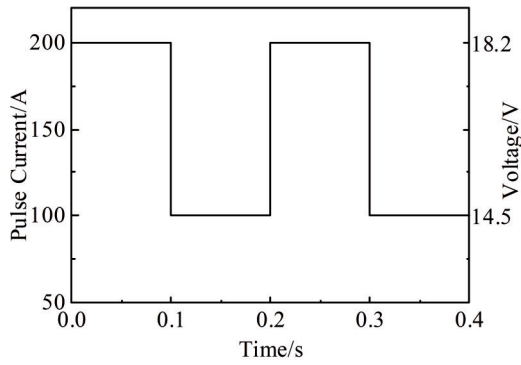


Fig.3 Variation of pulse current and voltage with time

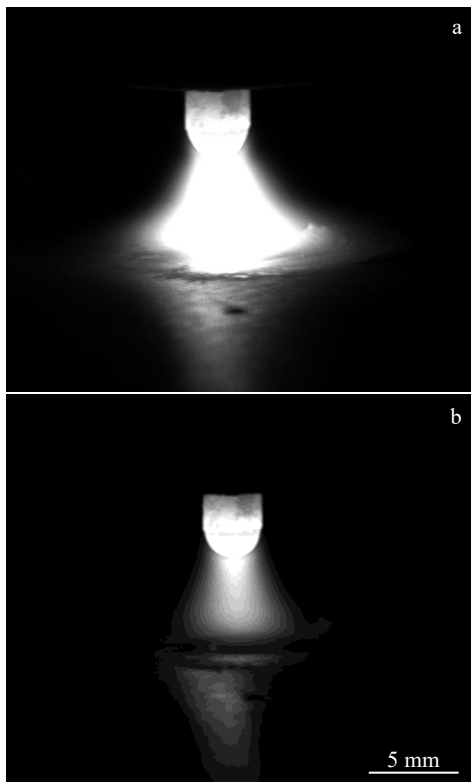


Fig.4 Arc shapes at peak current of 200 A (a) and base current of 100 A (b)

2 Results and Discussion

The cross-section of the molten pool was obtained along the longitudinal and transverse directions through the arc center. The 3D evolution process of the flow and temperature field in the molten pool can be observed and analyzed, as shown in Fig.5 and Fig.6.

It can be seen that when the pulse current and voltage switch from the peak state to the base state, the flatness of molten pool surface is restored due to the sudden decrease in the arc pressure. Since the xz plane is set as the symmetry boundary and the arc scanning is along the x -axis, the weld pool morphology and the surface ripples are symmetrically distributed. The temperature field distribution and the welding

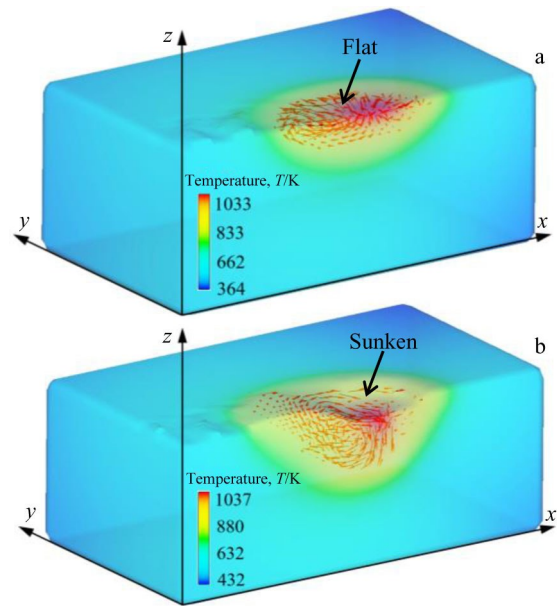


Fig.5 3D longitudinal cross-section of molten pool under different conditions: (a) $I=100$ A, $t=2.0$ s; (b) $I=200$ A, $t=3.5$ s

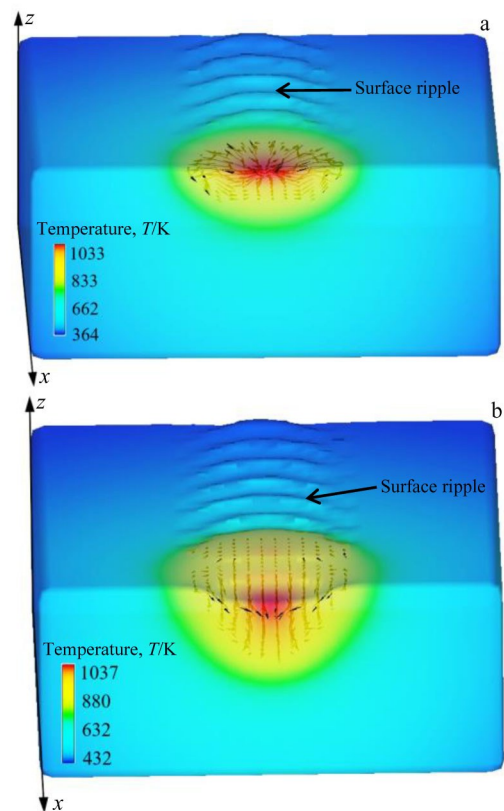


Fig.6 3D transverse cross-section of molten pool under different conditions: (a) $I=100$ A, $t=2.0$ s; (b) $I=200$ A, $t=3.5$ s

ripple morphology of the longitudinal cross-section through the arc center of molten pool are shown in Fig. 7. The maximum arc scanning velocity v_{max} is also shown in Fig.7.

When the arc scanning velocity v is set as 4 mm/s, the formation of surface ripples is more obvious. The solid

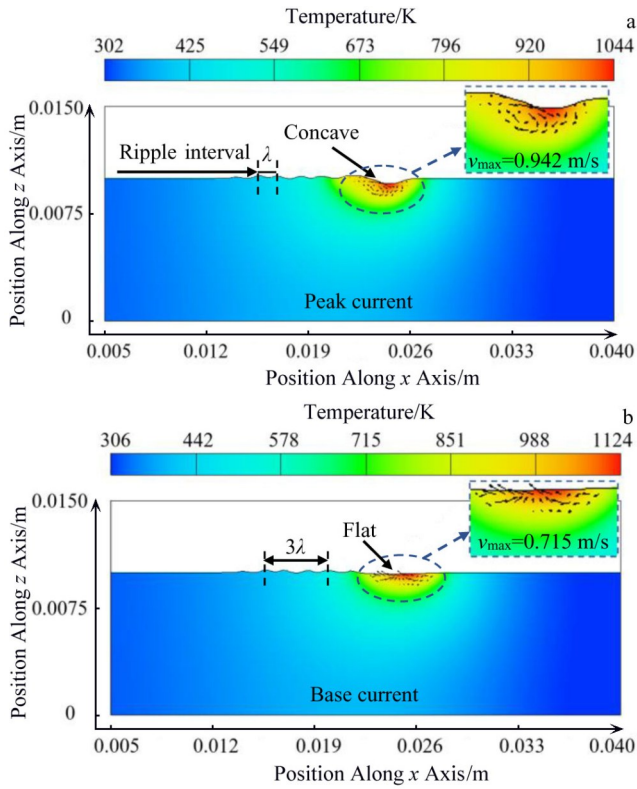


Fig.7 Temperature field distributions and welding ripple morphologies of longitudinal cross-section through arc center of molten pool under different conditions: (a) $I=200$ A, $t=1.25$ s; (b) $I=100$ A, $t=1.40$ s

fraction distribution during welding ripple formation is shown in Fig.8.

As shown in Fig.8, the solid phase fraction is 0.000 in the blue area, i.e., the blue area represents the liquid phase; the solid phase fraction is 1.000 in the red area, i.e., the red area represents the solid phase; other colors represent the mixed

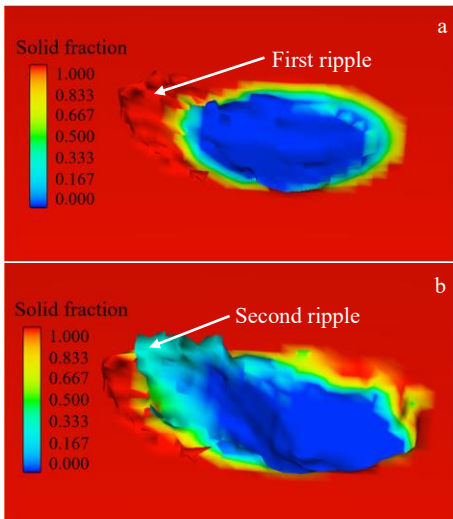


Fig.8 Distributions of solid phase fraction during the first ripple formation (a) and the second ripple formation (b)

phases. According to Eq. (4), the arc pressure is increased rapidly when the pulse current is switched to the peak value, resulting in the aggravation of surface depression of the molten pool. Consequently, the high-temperature fluid is pressed to the rear side of the arc scanning. When the high-temperature fluid is in contact with the previously formed welding wave, partial solidified area of the previously formed welding wave is re-melted, and the morphology changes slightly. The temperature of the molten pool center during the cooling process is shown in Fig.9. The temperature drops rapidly as the arc moves away, and rises slightly when the pulse current switches to peak state. The molten pool is completely solidified within 0.5 s, and the welding ripple remains on the substrate surface. The above process is repeated until the end of welding process.

The scanning speed of arc heat source affects the heat flux on the substrate surface, which is the main factor influencing the maximum depth of molten pool and the welding ripple space. The effect of arc scanning velocity on the weld pool depth and the spacing of adjacent welding ripples is shown in Fig.10.

Since one welding ripple forms in one current pulse period, the forming frequency of the welding ripples is equal to the current pulse frequency. Therefore, the distance between the adjacent welding ripples is approximately equal to the product of the arc scanning velocity and the pulse frequency. The

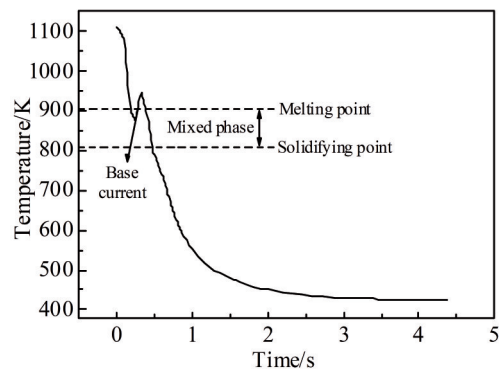


Fig.9 Temperature of molten pool center during cooling process

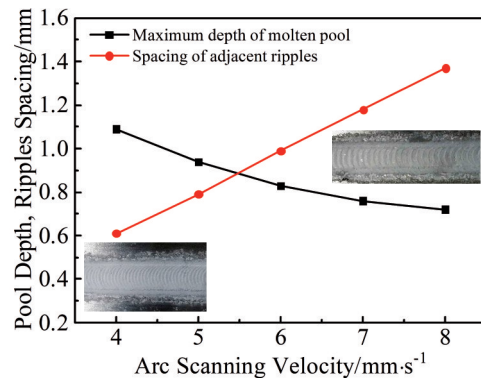


Fig.10 Effect of arc scanning velocity on weld pool depth and spacing of adjacent ripples

experiment platform was built to verify the calculation results of the weld pool depth and the spacing between welding waves, as shown in Fig. 11. The laser acted as the light compensation for shooting.

After the solidification of molten pool, the longitudinal cross-section of the molten pool is obtained. The molten pool depth (h) and distance between adjacent welding ripples (λ) with the arc scanning velocity $v=8$ mm/s are shown in Fig. 12. In order to reduce the experiment error, the value of twice the welding ripple spacing was used for statistical analysis. The experimental and calculated λ is 1.33 and 1.38 mm, respectively, and the error is 3.7%. The experimental and calculated h is 0.77 and 0.72 mm, respectively, and the error is 6.4%. The calculated and experimental results of λ and h at different arc scanning velocities are shown in Table 2. It can be seen that the maximum error between the calculation and

experiment results is 5.17%, which indicates that the theoretical analysis is reliable.

3 Conclusions

1) The arc driving forces are considered in the calculation model, including the surface tension, drag force, arc pressure, buoyancy, and Lorentz force. The formation of welding ripple is mainly caused by the periodic fluctuation of weld pool surface, which results from the arc forces and the rapid solidification of weld pool after arc scanning.

2) The molten pool surface fluctuates periodically when the pulse current is switched between the base state and the peak state, because of the sudden change of arc pressure.

3) The formation frequency of welding ripples is equal to the current pulse frequency. The distance between adjacent welding ripples is approximately equal to the product of the arc scanning velocity and the pulse frequency.

References

- 1 Ba Xianli, Gao Zeng, Wang Zhenjiang et al. *Rare Metal Materials and Engineering*[J], 2021, 50(10): 3657 (in Chinese)
- 2 Fande A W, Taiwade R V, Raut L. *Materials and Manufacturing Processes*[J], 2022, 37(8): 841
- 3 DebRoy T, Wei H L, Zuback J S et al. *Progress in Materials Science*[J], 2018, 92: 112
- 4 Babu S S, Raghavan N, Raplee J et al. *Metallurgical and Materials Transactions A*[J], 2018, 49(9): 3764
- 5 Unni A K, Vasudevan M. *Materials Today: Proceedings*[J], 2020, 27(3): 2768
- 6 Sharma A, Singh P K, Sharma R. *IOP Conference Series: Materials Science and Engineering*[C]. Mathura: IOP Publishing, 2021, 1116(1): 12 117
- 7 Huang J K, Liu G Y, He J et al. *Welding in the World*[J], 2021, 65(12): 2437
- 8 Chen B Q, Soares C G. *Marine Structures*[J], 2021, 75: 102 824
- 9 Sagar P, Gope D K, Chattopadhyaya S. *IOP Conference Series: Materials Science and Engineering*[C]. Sikkim: IOP Publishing, 2018, 377(1): 12 113
- 10 Mohanty U K, Sharma A, Abe Y et al. *Case Studies in Thermal Engineering*[J], 2021, 25: 100 885
- 11 Meng X M, Qin G L, Zou Z D. *International Journal of Heat and Mass Transfer*[J], 2017, 107: 1119
- 12 Wang D Q, Lu H. *International Journal of Heat and Mass Transfer*[J], 2021, 165: 120 572
- 13 Cho W I, Na S J. *Welding in the World*[J], 2021, 65(9): 1735
- 14 Zhao G X, Du J, Wei Z Y et al. *Journal of the Brazilian Society of Mechanical Sciences and Engineering*[J], 2019, 41(1): 1
- 15 Wei P S, Wu C K, Huang S K et al. *Science and Technology of Welding and Joining*[J], 2020, 26(1): 20
- 16 Liu J W, Rao Z H, Liao S M et al. *International Journal of Heat and Mass Transfer*[J], 2015, 91: 990
- 17 Liang R, Luo Y. *Optics & Laser Technology*[J], 2017, 93: 1

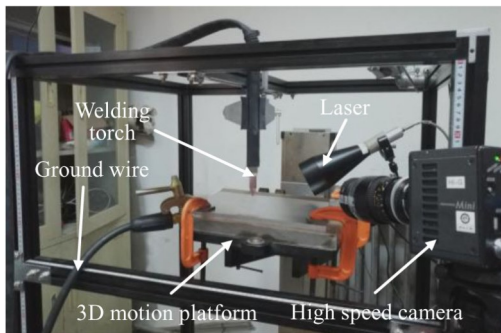


Fig.11 Appearance of experiment platform

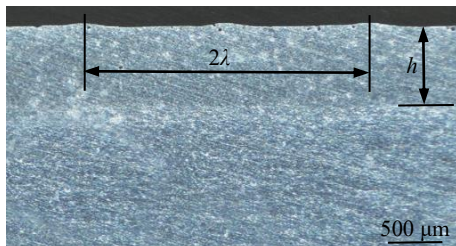


Fig.12 Longitudinal cross-section of molten pool

Table 2 Comparison between calculation and experiment results of molten pool depth h and distance between adjacent welding ripples λ

Arc scanning velocity/mm·s ⁻¹	Parameter	Calculation/mm	Experiment/mm	Error/%
4	λ	1.09	1.14	4.39
	h	0.61	0.58	5.17
5	λ	0.94	0.91	3.30
	h	0.79	0.82	3.66
6	λ	0.83	0.86	3.49
	h	0.99	0.96	3.13
7	λ	0.76	0.73	4.11
	h	1.18	1.23	4.07

- 18 Yao P, Zhou K, Tang H Q. *Materials*[J], 2019, 12(17): 2767
- 19 Zhou X M, Zhang H O, Wang G L et al. *International Journal of Heat and Mass Transfer*[J], 2016, 103: 521
- 20 Rao Z H, Zhou J, Liao S M et al. *Journal of Applied Physics*[J], 2010, 107(5): 54 905
- 21 Hu Y, Wang L, Yao J H et al. *Surface and Coatings Technology* [J], 2020, 383: 125 198
- 22 Ma Yan, Xu Yanze, Wang Jianju. *Rare Metal Materials and Engineering*[J], 2018, 47(9): 2621
- 23 Gu Y, Li Y D, Yong Y et al. *Welding in the World*[J], 2019, 63(2): 365
- 24 Campbell S W, Galloway A M, McPherson N A. *Science and Technology of Welding and Joining*[J], 2013, 18(7): 597
- 25 Han S W, Cho W I, Na S J et al. *Welding in the World*[J], 2013, 57(2): 257
- 26 Ikram A, Chung H. *Journal of Manufacturing Processes*[J], 2021, 64: 1529
- 27 Komen H, Shigeta M, Tanaka M. *International Journal of Heat and Mass Transfer*[J], 2018, 121: 978
- 28 Yang Ziyou, Fang Yuchao, He Jingshan. *Rare Metal Materials and Engineering*[J], 2021, 50(3): 881 (in Chinese)

交流脉冲 TIG 焊波成形过程数值分析

赵光喜^{1,2,3}, 程 祥¹, 杨先海¹, 郑光明¹, 刘焕宝¹, 谭 帅²

(1. 山东理工大学 机械工程学院, 山东 淄博 255000)

(2. 胜利油田高原石油装备有限责任公司, 山东 东营 257091)

(3. 山东省精密制造与特种加工重点实验室, 山东 淄博 255000)

摘 要: 考虑到电弧驱动力的影响, 建立了在交流脉冲钨惰性气体 (TIG) 焊过程中焊波成形的三维瞬态数值分析模型。为避免焊丝熔化成熔滴后对电弧熔池表面波动的影响, 当电弧在 2024 铝合金基板上扫描时, 送丝机不送丝。结果表明, 当电流在基值与峰值之间切换时, 熔池表面呈周期性的波动, 且随着电弧的移动, 熔池后沿逐渐凝固。在大温度梯度下冷却的熔池表面在恢复平整前就已经凝固, 从而形成焊波。焊波形成频率与电流脉冲频率相同, 且相邻焊波间距约等于电弧扫描速度与电流脉冲频率的乘积。

关键词: 焊波形成; TIG 焊; 熔池; 电弧驱动力

作者简介: 赵光喜, 男, 1989 年生, 博士, 山东理工大学机械工程学院, 山东 淄博 255000, E-mail: zgx2019@sdut.edu.cn